Check for updates

Geochemistry, Geophysics, Geosystems®

AGU ADVANCING EARTH AND SPACE SCIENCES

RESEARCH ARTICLE
10.1029/2024GC011680

# Zircon Constraints on the Eruptive Sequence and Magma Evolution of Rhyolites at South Sister Volcano, Oregon

**Annika E. Dechert[1], Nathan L. Andersen[2], Josef Dufek[1], and Christine E. Jilly[3]**

[1]Department of Earth Sciences, University of Oregon, Eugene, OR, USA, [2]U.S. Geological Survey, Cascades Volcano Observatory, Vancouver, WA, USA, [3]Department of Earth & Planetary Sciences, Stanford University, Stanford, CA, USA

**Key Points:**

- Zircon ages shift inferred eruption ages for two South Sister rhyolites over 10 kyr younger
- Crystallization of zircon and plagioclase as well as destabilized amphibole and titanite leveraged melt compositions of Pleistocene magmas
- Compositional distinctions between the Pleistocene and Holocene lavas suggest distinct melt sources for both eruption sequences

**Supporting Information:**

Supporting Information may be found in the online version of this article.

**Correspondence to:**

A. E. Dechert,
adechert@uoregon.edu

**Citation:**

Dechert, A. E., Andersen, N. L., Dufek, J., & Jilly, C. E. (2024). Zircon constraints on the eruptive sequence and magma evolution of rhyolites at South Sister volcano, Oregon. *Geochemistry, Geophysics, Geosystems*, *25*, e2024GC011680. https://doi.org/10.1029/2024GC011680

Received 23 MAY 2024
Accepted 2 AUG 2024

© 2024 The Author(s). Geochemistry, Geophysics, Geosystems published by Wiley Periodicals LLC on behalf of American Geophysical Union.
This is an open access article under the terms of the Creative Commons Attribution-NonCommercial-NoDerivs License, which permits use and distribution in any medium, provided the original work is properly cited, the use is non-commercial and no modifications or adaptations are made.

**Abstract** We present $^{230}$Th-$^{238}$U crystallization ages and trace element compositions for zircons spanning the late Pleistocene to Holocene rhyolite eruptive record at South Sister volcano in the central Oregon Cascade Range. Most zircon ages are between 100 and 20 ka, with very few in secular equilibrium (>350 ka). The weighted mean of zircon ages for the two oldest South Sister rhyolites, 31.5 ± 2.1 and 39.1 ± 2.4 ka, are significantly younger than the associated $^{40}$Ar/$^{39}$Ar ages, 47.4 ± 9.7 and 51.4 ± 9.7 ka. We propose that these $^{40}$Ar/$^{39}$Ar dates, performed on plagioclase separates, are compromised by a subtle amount of excess Ar and therefore the younger weighted mean zircon ages yield more reliable eruption ages. These results imply that the interval of rhyolite eruption at South Sister during the late Pleistocene was both shorter and more productive than previously thought and that eruption at South Sister initiated after Middle Sister. Compositionally, zircons from the Pleistocene rhyolites are broadly similar and show down-temperature zircon and plagioclase crystallization trends. However, we argue that destabilized amphibole and titanite in a common mush also exert leverage on the Pleistocene zircon trace element compositions. Divergence in the Eu/Eu* ratio between the Pleistocene and Holocene lavas implies chemically distinct magma reservoirs originating from the Pleistocene rhyolite eruptive sequence and the Holocene eruptive sequence. This work suggests a higher flux of rhyolite volcanism than previously thought and characterizes magmatic storage distinctions between the Pleistocene and Holocene rhyolites, aiding in the assessment of future eruptive hazards at South Sister volcano.

## 1. Introduction

Globally, small volume but frequent explosive volcanic eruptions impact populations and aviation due to eruptive plumes, ashfall, lava flows, and lahars. Therefore, continuing interdisciplinary research at active volcanoes will help inform hazard assessments and mitigation strategies for future eruptions (e.g., Ewert et al., 2018). Geologic and petrologic approaches offer complimentary views of past eruptions and their implications for future behavior. On one hand, geologic studies yield information about the frequency, magnitude, and style of past activity to assess plausible future eruption scenarios. On the other hand, petrologic methods provide an understanding of how the magmatic system has evolved and may offer clues about which past eruptions are more likely to be representative of the modern system and future behavior. The mineral zircon provides coupled temporal and compositional information that can inform both the timing of past eruptions and the evolution of the underlying magmatic system.

The utility of zircon is due to its durability, high compatibility with elements useful for geochronology and petrology (e.g., U, Th, and the rare earth elements (REE)), and a well-characterized temperature dependence of saturation (Finch & Hanchar, 2003; Hoskin & Schaltegger, 2003; Watson & Harrison, 1983). Zircon petrochronology has been applied to large eruptive volume systems (Reid et al., 1997; Rubin et al., 2017; Simon & Reid, 2005) as well as small to medium eruptive volume systems (e.g., Claiborne et al., 2010) to distinguish chemical, thermal, spatial, and temporal characteristics of melt evolution and processes (Cooper, 2015). In the Cascade Range, zircon studies have informed models of magma evolution and storage at Mount St. Helens (e.g., Claiborne et al., 2010), South Sister (e.g., Stelten & Cooper, 2012), Crater Lake (e.g., Bacon & Lowenstern, 2005), and Lassen Peak (e.g., Klemetti & Clynne, 2014). However, the dearth of rhyolite and lower U in these arc magmas has, in part, hindered broader application of zircon geochronology in the Cascade Range (Hildreth, 2007). The previous zircon study at South Sister focused only on the most recent eruptions (Stelten & Cooper, 2012); however, the rhyolites that erupted in the late Pleistocene remain little investigated.

The U.S. Geological Survey has classified the Three Sisters volcanic complex as a "very high threat potential" to the surrounding communities, such as Bend (pop. 100,000), only 50 km away (Ewert et al., 2018). Past eruptions

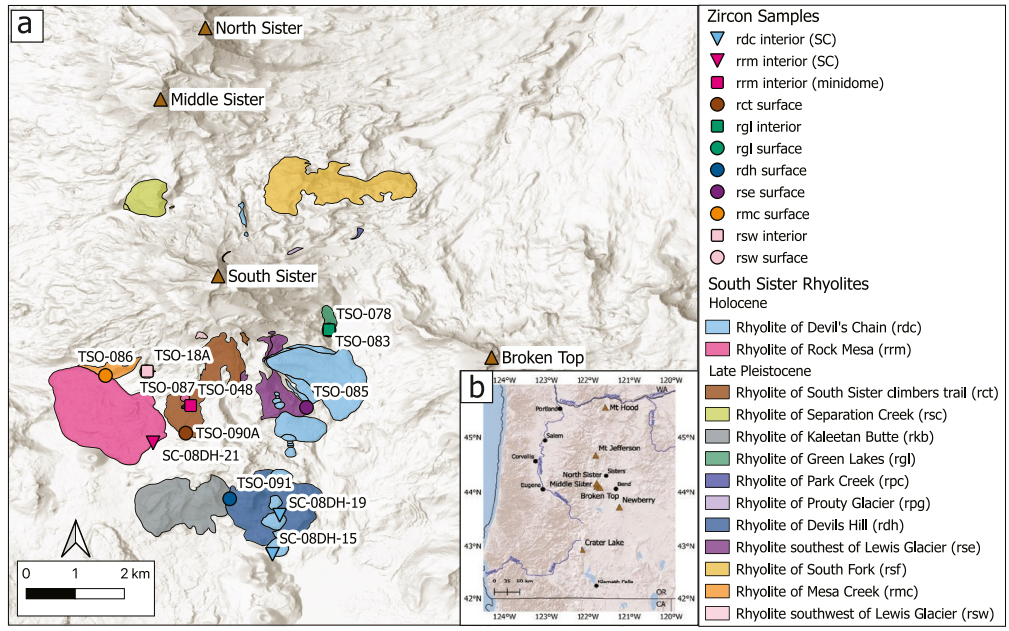


**Figure 1.** (a) Simplified geologic map of the South Sister rhyolites (modified from Hildreth et al., 2012) with the locations of samples discussed in this paper. Brown triangles show South Sister, Middle Sister, North Sister, and Broken Top summits. Cyan and magenta triangles denote the samples of Stelten and Cooper (2012). Squares symbolize zircon interior analysis and circles symbolize zircon surface analyses for samples from this study. Colors signify samples from the same eruptive unit. See Dechert (2024) or supplemental data for sample coordinates. (b) Inset shows the location of the Three Sisters in the Oregon Cascade Range, other notable Cascade Range volcanoes, and major cities.

included hazards such as pyroclastic density currents, lava flows, and ash plumes (Scott et al., 2001). South Sister volcano has erupted approximately 12 $km^3$ of volcanic rocks over its lifetime, including 13 rhyolitic eruptions ranging from 51 to 2 ka (Fierstein et al., 2011; Hildreth et al., 2012). Frequent eruption of rhyolite and its modest eruptive volume make South Sister an ideal system to investigate the origin and pre-eruptive storage of rhyolite in smaller volume magmatic systems.

In addition to the recent eruptions, South Sister has experienced ground inflation since the mid-1990s focused 5 km west of the summit and only ~3 km from the late Holocene Rhyolite of Rock Mesa (rrm) vent (Lisowski et al., 2021). InSAR, continuous GPS, leveling, and modeling studies proposed multiple mechanisms of this uplift including the continuing intrusion of basaltic magma (hydraulic), a delayed response of visco-elastic crust to a past magma intrusion (viscoelastic), or the pressurizing of a geothermal system (poroelastic) (Dzurisin et al., 2009; Riddick & Schmidt, 2011; Wicks et al., 2002). These studies suggest that the source of deformation is approximately 5–7 km deep. Additionally, a study of springs near South Sister found He and C isotope ratios and elevated heat flow consistent with contributions from mafic magma (Evans et al., 2004). As such, the working hypothesis suggests an intrusion of basaltic magma 5–7 km below South Sister. This intrusion could lead to a future eruption at South Sister, and understanding how the past magmatic system compares to the modern system can help inform eruption and hazard forecasting.

We present $^{230}Th$-$^{238}U$ crystallization ages and trace element compositions of zircon crystals from rhyolites at South Sister volcano. Results of this study suggest (a) South Sister hosted a long-lived magmatic system primed for zircon crystallization from 100 to 20 ka, (b) the earliest rhyolite eruptions were more than 10 kyr younger than past studies suggested, (c) South Sister was characterized by a high eruption rate from 40–30 ka, and (d) the Pleistocene and Holocene rhyolites were derived from chemically distinct sources.

## 2. Geologic Background

The Three Sisters volcanic complex comprises three stratovolcanoes (North Sister, Middle Sister, and South Sister) located in the central Oregon Cascade Range, USA (Figure 1). The regional tectonics of this reach of the



15252027, 2024, 8, Downloaded from https://agupubs.onlinelibrary.wiley.com/doi/10.1029/2024GC011680, Wiley Online Library on [02/02/2025]. See the Terms and Conditions (https://onlinelibrary.wiley.com/terms-and-conditions) on Wiley Online Library for rules of use; OA articles are governed by the applicable Creative Commons License

15252027, 2024, 8, Downloaded from https://agupubs.onlinelibrary.wiley.com/doi/10.1029/2024GC011680, Wiley Online Library on [02/02/2025]. See the Terms and Conditions (https://onlinelibrary.wiley.com/terms-and-conditions) on Wiley Online Library for rules of use; OA articles are governed by the applicable Creative Commons License

Cascade Range is complicated by the interaction between the warm Cascadia subduction zone, the past influence of the Yellowstone plume, the edge of the Basin and Range extension, and may contribute to the unusual abundance of high-$SiO_2$ volcanism for this region of the Cascade Range (C. Cheng et al., 2017; McCrory et al., 2012; Obrebski et al., 2010). The oldest and northernmost of the three, the North Sister, erupted basaltic andesite with major cone construction from approximately 120–45 ka (Hildreth et al., 2012; Schmidt & Grunder, 2009). Growth of Middle Sister occurred from approximately 49–15 ka with compositions ranging from basaltic andesite to rhyolite (Calvert et al., 2018). The building of the South Sister edifice alternated between rhyolite and intermediate products from ∼51–22 ka, largely coevally with the Middle Sister (Fierstein et al., 2011). The growth of all the Three Sisters stratovolcanoes was preceded by the growth of Broken Top stratovolcano, located just 5 km southeast of South Sister. Broken Top erupted 7–10 $km^3$ of basaltic andesite to rhyodacite from approximately 300–150 ka (Hildreth, 2007). In total, the Three Sisters reach of the Cascade Range extends 90 km N-S in Central Oregon, and has at least 466 Quaternary volcanoes (Hildreth, 2007). Postglacial mafic eruptions are more common in this area than elsewhere in the Cascade Range. These postglacial volcanic centers include the Sand Mountain volcanic field, Blue Lake volcano, LeConte Crater, Fish Lake lava from Nash Crater, Lost Lake cones, Four In One Cone, Yapoah Crater, Collier Cone, and Belknap Crater (Sherrod et al., 2004). Slightly farther south lies Mount Bachelor, which is the largest of approximately 50 N-S aligned basalt to basaltic andesite vents that erupted from 18–8 ka (Gardner, 1994).

The eruption chronology at Three Sisters has largely been established by $^{40}Ar/^{39}Ar$ dates (Calvert et al., 2018; Fierstein et al., 2011; Hildreth et al., 2012). However, Fierstein et al. (2011) used the Taylor Creek sanidine standard age of 27.87 Ma while Calvert et al. (2018) used a more recently determined, slightly older age for the Taylor Creek sanidine standard of 28.345 Ma (Fleck et al., 2019). To ensure that all the $^{40}Ar/^{39}Ar$ dates are reported on the same basis and are directly comparable, we have recalculated the $^{40}Ar/^{39}Ar$ dates using the ArAR software of Mercer and Hodges (2016) to an updated Taylor Creek age of 28.447 Ma (equivalent to a Fish Canyon Sanidine age of 28.201 Ma; Fleck et al., 2019; Schaen et al., 2021) and decay constants of Min et al. (2000). For the remainder of this paper, we will report $^{40}Ar/^{39}Ar$ ages for South Sister based on this recalculation (Figure S1 in Supporting Information S1).

South Sister's eruptive history highlights a range of compositions and one of the rare instances of rhyolite in the Cascade Range (Hildreth, 2007). The oldest exposed lava at South Sister is rhyolitic at 51.4 ± 9.7 ka and eruptions alternated between rhyolitic, dacitic, and andesitic through ∼37 ka (Fierstein et al., 2011). Then, a broad cone composed of andesitic to dacitic lava grew from 37 to 30 ka. Activity became concentrated at a the summit cone by ∼27 ka culminating with the final and most mafic South Sister eruption at ∼22 ka, which formed the present-day summit crater (Fierstein et al., 2011). Finally, two rhyolitic eruptions occurred at approximately 2 ka on the SW and E flanks of the volcano (Scott, 1987). Previous studies have hypothesized that the mechanism for rhyolite production at South Sister could include (a) partial melting from different crustal compositions, (b) fractional crystallization from mafic precursor magma, or (c) the Holocene rhyolites could reflect the rejuvenation of residual rhyolitic magmas related to the late Pleistocene eruptions (Brophy & Dreher, 2000; Calvert et al., 2018; Fierstein et al., 2011; Hill, 1991; Parker et al., 2023; Waters et al., 2021). Hypotheses to explain the compositional gaps in the suite of Three Sisters eruptive products include fractional crystallization (Brophy & Dreher, 2000; Dufek & Bachmann, 2010) and partial melting (Waters et al., 2021); however, these gaps are not as dramatic at South Sister when considering the more comprehensive data set of Hildreth et al. (2012). These hypotheses highlight the importance of further study as the mechanisms of silicic magma genesis at South Sister and the connection between the late Pleistocene and Holocene rhyolite eruptive episodes remain an open question.

Zircon and plagioclase geochronology and trace element chemistry of the two Holocene rhyolite eruptions suggest two distinct magma sources. rrm erupted at 2,150 ± 150 $^{14}C$ yr B.P. (preferred $^{14}C$ age of Scott, 1987) with a main coulee, pumice-fall deposits, and satellite domes on the SW flank of South Sister (Hildreth et al., 2012; Scott, 1987). Rhyolite of Devils Chain (rdc) erupted at 2,000 ± 200 $^{14}C$ yr B.P. in a series of seven lava flows and domes aligned N-S on the southeast flank of South Sister (Hildreth et al., 2012; Scott, 1987). Here, we note different naming of units between sources but consider them superseded by Hildreth et al. (2012). The zircon $^{230}Th$-$^{238}U$ crystal ages are predominantly 80–20 ka for both Holocene eruptions with a small number of grains in secular equilibrium (>350 ka) (Stelten & Cooper, 2012). The zircon crystals with resolvable dates are interpreted to be antecrystic, inherited from the longer-lived system (Stelten & Cooper, 2012). Conversely, bulk plagioclase $^{230}Th$-$^{226}Ra$ crystal ages trend closer to eruption age, 6.8–2.3 ka for rrm and 9.6–4.0 ka for rdc (Stelten & Cooper, 2012). The Ti-in-zircon geothermometer indicates that zircon crystallization ranges from 640

15252027, 2024, 8, Downloaded from https://agupubs.onlinelibrary.wiley.com/doi/10.1029/2024GC011680, Wiley Online Library on [02/02/2025]. See the Terms and Conditions (https://onlinelibrary.wiley.com/terms-and-conditions) on Wiley Online Library for rules of use; OA articles are governed by the applicable Creative Commons License

to 837°C (Stelten & Cooper, 2012). The distinct trace element ratio of Hf/Nb in the rrm and rdc zircon crystals suggests that these eruptions were sourced from two chemically and physically distinct reservoirs that coexisted temporally in the broader, shared magmatic system (Stelten & Cooper, 2012). While this work focused on the Holocene rhyolites, no such work has included the late Pleistocene South Sister rhyolites.

## 3. Samples and Methods

Samples collected for this work include six late Pleistocene and one Holocene rhyolite from South Sister (Figure 1). The units span the southern spatial extent of the rhyolite eruptions and the known eruption age range. Zircon data were collected for the Rhyolite southwest of Lewis Glacier (rsw), Rhyolite of Mesa Creek (rmc), Rhyolite of southeast Lewis Glacier (rse), Rhyolite of Devils Hill (rdh), Rhyolite of Green Lakes (rgl), and Rhyolite of South Sister clumbers trail (rct). These units erupted between 51.4 and 24 ka based on $^{40}Ar/^{39}Ar$ ages reported by Fierstein et al. (2011), Hildreth et al. (2012), and Calvert et al. (2018). Ages are based on incremental heating of plagioclase separates (rsw, rmc, and rct) or groundmass (rse, rdh, rgl) separates. Of the Pleistocene rhyolites, rse, rgl, rdh, and rdc are on the southeastern flank of the volcano, which situates them near Broken Top. Our work also considers the Holocene rrm and rdc rhyolites that erupted at 2,150 ± 150 $^{14}C$ yr B.P. and 2,000 ± 200 $^{14}C$ yr B.P. These eruption ages are based on $^{14}C$ dates of wood fragments within rrm pumice fall and a soil directly underlying rdc tephra (Scott, 1987). We collected a sample of ejecta associated with the rrm satellite minidomes and compared our results to those of Stelten and Cooper (2012) samples from the main rrm coulee and two of the southern rdc domes (Figure 1).

Zircon separates were produced by Zirchron LLC using standard magnetic and density separation techniques including crushing, electro pulse disaggregation, water table, heavy liquids, and Frantz. Analysis of $^{238}U$-$^{230}Th$ dates and trace element compositions were conducted on the SHRIMP-RG (reverse geometry) ion microprobe co-operated by U.S. Geological Survey and Stanford University in the SUMAC facility at Stanford University during multiple sessions in 2023. Zircons were pressed into indium mounts and left unpolished. For these surface analyses, trace element data were collected followed by $^{230}Th$-$^{238}U$ analysis on the same spot. We also attempted to measure zircon interiors by mounting them in epoxy and polishing the mount. A cathodoluminescence image of the polished interiors displays the size, shape, and textures of the crystals analyzed (Figure S2 in Supporting Information S1). The average c-axis is 87 μm and the average a-axis is 49 μm. Crystals are euhedral and the most common shape is equant with additional shapes being tabular and prismatic. Approximately 30% of the crystals exhibit sector zoning, another 30% have patchy zoning, with oscillatory, homogeneous, diffuse, and irregular patters for the rest. One sample, rrm minidome, does include resorbed cores in 6 of the 22 crystals analyzed. Unfortunately, the small size of most of the zircon crystals frequently resulted in the beam impinging on the epoxy during $^{230}Th$-$^{238}U$ analysis of crystal interiors yielding a significant carbide interference and unusable data.

The U-Th analytical procedure and data reduction procedures follow the methods developed by Williams (1997) and Ireland and Williams (2003). An $O_2^-$ primary beam with an accelerating voltage of 10 kV was used to sputter secondary ions from the sample surface with a 15–16 nA primary beam current focused to a ~37 μm spot. Seven masses were measured, including $^{90}Zr_2{}^{16}O$, $^{238}U^+$, $^{232}Th^{12}C^+$, $^{230}Th^{16}O^+$, background measured 0.050 AMU above the $^{230}Th^{16}O^+$ peak, $^{232}Th^{16}O^+$, and $^{238}U^{16}O^+$. Data were collected over 8 scans per spot, for a total run time of ~30 min, collected by magnet peak-jumping on an electron multiplier. Zircon U concentration data were standardized against the well-characterized MAD-559 zircon standard (3,940 ppm U (Coble et al., 2018)).

For trace element analyses, an $O_2^-$ primary beam with accelerating voltage of 10 kV was used to sputter secondary ions from the sample surface with a 1.5 nA primary beam current focused to a ~16 μm spot. The acquisition included analysis of 29 masses, all measured by peak jumping on an electron multiplier: $^{28}Si^{16}O^+$, $^{45}Sc^+$, $^{48}Ti^+$, $^{49}Ti^+$, $^{56}Fe^+$, $^{89}Y^+$, $^{93}Nb^+$, $^{92}Zr^1H^+$, $^{96}Zr^+$, $^{139}La^+$, $^{140}Ce^+$, $^{141}Pr^+$, $^{146}Nd^+$, $^{147}Sm^+$, $^{153}Eu^+$, $^{155}Gd^+$, $^{165}Ho^+$, $^{159}Tb^{16}O^+$, $^{162}Dy^{16}O^+$, $^{166}Er^{16}O^+$, $^{169}Tm^{16}O^+$, $^{172}Yb^{16}O^+$, $^{175}Lu^{16}O^+$, $^{90}Zr_2{}^{16}O^+$, $^{180}Hf^{16}O^+$, $^{206}Pb^+$, $^{207}Pb^+$, $^{232}Th^{16}O$, and $^{238}U^{16}O^+$. Count times ranged from 2 to 18 s per mass to optimize counting statistics for each isotope, for a total run time of ~13 min per spot. See Text S1 in Supporting Information S1 for additional details of the SHRIMP-RG analytical methods.

Zircon ages are calculated using the decay constant of H. Cheng et al. (2013) and the method of Boehnke et al. (2016). The Boehnke et al. (2016) method calculates a date based on a mode equilibrium melt for each zircon spot based on the $^{238}U/^{232}Th$ measured in the zircon, an assumed U/Th partition coefficient ratio between the

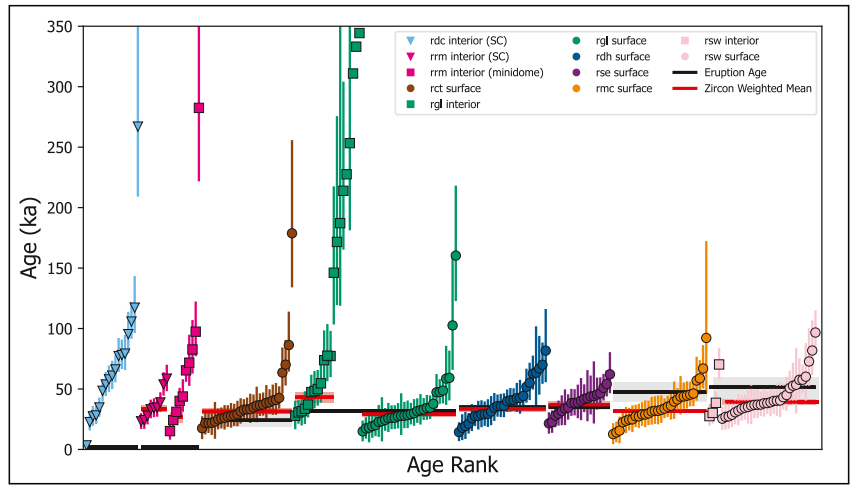


**Figure 2.** Rank order plot of zircon crystallization ages. Data of Stelten and Cooper (2012) symbolized as triangles and labeled (SC). Zircon surface analyses are circles and interior analyses are squares. Black horizontal lines with gray fields show the associated $^{14}$C date (rdc and rrm) or $^{40}$Ar/$^{39}$Ar date (all others) with 1$\sigma$ uncertainty (Fierstein et al., 2011; Scott, 1987). Red horizontal lines with salmon fields show the zircon weighted mean date with 1$\sigma$ uncertainty of the youngest group of zircons that yield an acceptable mean square weighted deviation. Note that the zircon weighted mean age for rmc and rsw are younger than the $^{40}$Ar/$^{39}$Ar date at 1$\sigma$. Geologic unit abbreviations are as in Figure 1.

zircon and the melt, and assumes that melt variance from the equiline is ±15% (1$\sigma$). We calculated this mean U/Th partition coefficient to be 5.4 ± 0.8 from the South Sister zircons and sample whole rock compositions (Table S4).

The dates reported by Stelten and Cooper (2012) for the Holocene rhyolites were calculated using a two-point model isochron approach (e.g., Reid et al., 1997) using the glass Th isotope ratios of the host rhyolites and the older decay constant of H. Cheng et al. (2000). To ensure our dates are comparable to those of Stelten and Cooper (2012), we first recalculated their model isochrons using the newer decay constant of H. Cheng et al. (2013) and found only a 5% average difference with the updated decay constant after removing one crystal in secular equilibrium. We then compared these dates to those calculated from their data using the Boehnke et al. (2016) model and employed for our measurements and found a 38% difference for rdc (59% absolute difference within uncertainty) and 30% for rrm (78% absolute difference within uncertainty). Stelten and Cooper (2012) found the Holocene rhyolite whole rock compositions to be in 2% Th-excess. This contrasts to the average of secular equilibrium ±15% that is assumed in the Boehnke et al. (2016) model and is a potential source of bias. We tested the magnitude of this bias by calculating model isochron dates using a whole rock Th isotope composition based on the whole rock U/Th ratio and assumptions of secular equilibrium and with 2% Th excess. We find that assuming 2% Th-excess makes an average difference of 2.2% in the calculated dates, which is less than the analytical uncertainty. In the absence of whole-rock or glass Th isotope compositions for the Pleistocene rhyolites, we prefer the method of Boehnke et al. (2016) and find that the assumption that the host melt is in secular equilibrium on average is simpler and no less reasonable than assuming that the Th-excess measured for the Holocene rhyolites was homogeneous throughout the magma system and unchanging during the interval of zircon crystallization. All zircon dates discussed in the rest of this paper were calculated by the Boehnke et al. (2016) model without Th excess. Additionally, to also ensure that the trace element measurements from Stelten and Cooper (2012) are comparable to the late Pleistocene data, we recalculated the Holocene data with preferred concentrations of Coble et al. (2018) that intercalibrate MAD-1 (standard of Stelten and Cooper (2012)) and MAD-559 (standard of this work) zircon trace element standards.

## 4. Results

### 4.1. Zircon $^{230}$Th-$^{238}$U Dates

Individual $^{230}$Th-$^{238}$U ages are model ages calculated using the Boehnke et al. (2016) model and represent zircon crystallization ages. Our data include 18 analyses in secular equilibrium, and thus unresolvable dates >350 ka. The 228 resolvable zircon dates range from 282.5–3.4 ka, but 199 (87%) are approximately 100–20 ka (Figure 2).



15252027, 2024, 8, Downloaded from https://agupubs.onlinelibrary.wiley.com/doi/10.1029/2024GC011680, Wiley Online Library on [02/02/2025]. See the Terms and Conditions (https://onlinelibrary.wiley.com/terms-and-conditions) on Wiley Online Library for rules of use; OA articles are governed by the applicable Creative Commons License

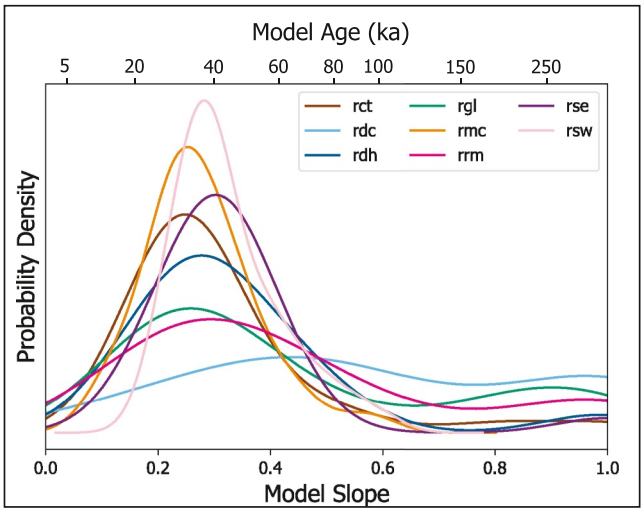


**Figure 3.** Probability density functions of the zircon populations by unit based on model isochron slope calculated by the method of Boehnke et al. (2016). Surface and interior data are combined for each unit. Geologic unit abbreviations are as in Figure 1.

There are three dates from rgl interiors that are nominally resolvable from 344.4–310.9 ka but are within error of secular equilibrium and therefore potentially older. The zircon dates for units rsw, rmc, rse, rdh, and rct all yield probability density maxima around 40 ka (Figure 3). Units rrm (combined) and rdc show a broad distribution with no distinct peaks. The unpolished surface analyses (rsw, rmc, rse, rdh, rgl, rct) yield a narrower range of younger dates compared to the crystal interiors (rdc, rrm coulee, rrm minidome, rgl, rsw). This is especially true for rgl interiors; however, we do not have a complete data set of interior and surface analyses for the other units. Unit rgl shows two populations of zircon ages, one between 100 and 20 ka, probability density maxima of ~40 ka, like the other Pleistocene rhyolites, and one >150 ka, probability density maxima of ~250 ka (Figure 3). The coherent >150 ka population was not found in the rgl surface dates or the surface dates of the other rhyolites. While we only have four interior analyses for rsw, the zircon crystal date range of 70.2–27.6 ka matches that of the larger surface data set, 96.7–25.4 ka.

In addition to individual zircon dates, we calculate weighted mean dates for the youngest distinguishable group of dates. We calculate this weighted mean age by including progressively older zircon crystal dates until the mean square weighted deviation (MSWD) exceeded the critical value. Given the spread of ages and the size of the data set, we are not able to calculate a zircon weighed mean age for rdc (Figure S4 in Supporting Information S1). The zircon weighted mean age for the rrm main flow, rrm minidome, rct, and rgl interiors are all older than the associated $^{40}Ar/^{39}Ar$ or $^{14}C$ dates. The zircon weighted mean dates for rgl surfaces, rdh, and rse are equivalent to the associated $^{40}Ar/^{39}Ar$ date. However, the zircon weighted mean dates for the rmc and rsw surface and rsw interior are younger than the associated $^{40}Ar/^{39}Ar$ dates at the $1\sigma$ level (Figure S4 in Supporting Information S1). The $^{40}Ar/^{39}Ar$ eruption date for rmc is $47.4 \pm 8.2$ ka and the zircon weighted mean date is $31.5 \pm 2.1$ ka ($n = 30$, MSWD = 1.02). The $^{40}Ar/^{39}Ar$ date for rsw is $51.4 \pm 9.7$ ka and the zircon weighted mean date for surfaces is $39.1 \pm 2.4$ ka ($n = 30$, MSWD = 0.89). For both rmc surfaces and rsw surfaces, the $^{40}Ar/^{39}Ar$ eruption date and the zircon weighted mean age are differentiated at $1\sigma$ confidence level, such that the propagated uncertainty of the difference is less than the difference, but not at the $2\sigma$ confidence level.

### 4.2. Compositional Trends

Nearly all the zircon crystals have U contents lower than 500 ppm (Figure S5 in Supporting Information S1); only 18 have higher concentrations up to 2,610 ppm. Ti concentrations cluster between 3 and 10 ppm, some reaching up into low to mid 20s ppm Ti (Figure 4). Eu/Eu* is generally low, ranging from 0.02 to 0.34 (Figure 4). Outside a few outliers, the Hf concentrations range between approximately 6,000 to 11,000 ppm.

Zircon Hf concentrations correlate with some trace elements. We see decreasing Ti concentrations and Eu/Eu* with increasing Hf concentrations (Figure 4, Figure S5 in Supporting Information S1). However, elements such as Y, Sc, Nb, and ratios such as U/Th are not correlated with Hf concentrations, producing sub-vertical arrays (Figure S5 in Supporting Information S1). These elements and ratios that do not correlate with Hf do show some correlation with each other. For example, higher ratios of U/Th correlate with higher ratios of Hf/Nb and Yb/Gd. There is no apparent correlation between zircon age and composition for any of the Pleistocene rhyolites (Figure 5).

### 4.3. Zircon Temperatures

Crystallization temperatures are calculated using zircon Ti concentrations and the Ti-in-zircon geothermometer calibration of Ferry and Watson (2007). This calibration requires activities of $SiO_2$ and $TiO_2$. However, determining these values is not straightforward for the South Sister rhyolites. We consider a range of these two activities, how those ranges impact the Ti-in-zircon temperature, and how phases in the South Sister system would impact these activities (see Text S1 in Supporting Information S1). The most reasonable assumptions are an activity of 1 for $SiO_2$ and 0.7 for $TiO_2$, and the zircon temperatures presented here use



15252027, 2024, 8, Downloaded from https://agupubs.onlinelibrary.wiley.com/doi/10.1029/2024GC011680, Wiley Online Library on [02/02/2025]. See the Terms and Conditions (https://onlinelibrary.wiley.com/terms-and-conditions) on Wiley Online Library for rules of use; OA articles are governed by the applicable Creative Commons License

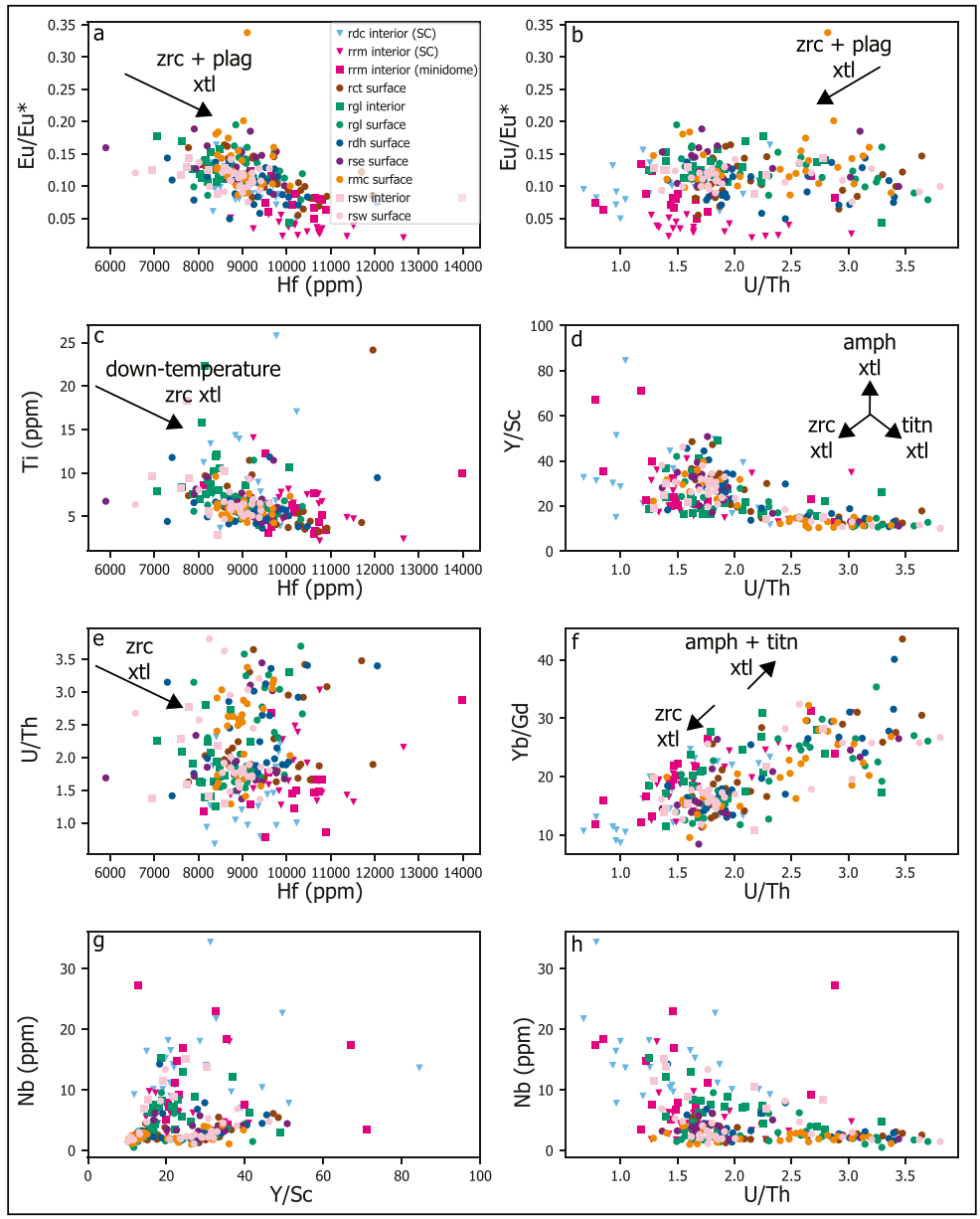


**Figure 4.** Variation of selected zircon trace elements and ratios. One anomalously high Hf/Nb ratio and Y/Sc ratio plots off scale. zrc = zircon, amph = amphibole, titn = titanite, xtl = crystallization. Geologic unit abbreviations are as in Figure 1.

these activities. The temperature range for all zircons spans from 647 to 855°C (Figure S6 in Supporting Information S1). The Pleistocene eruptions all show a similar average Ti-in-zircon temperature from 724 to 768°C (Figure S6 in Supporting Information S1). Of these Pleistocene units, rgl yields the highest average, while rmc and rdh show the coolest temperatures. For the Holocene rhyolites, rdc has the highest average temperature. Interestingly, rrm collected from the main coulee has a slightly higher average temperature than the sample we collected from the minidome ejecta (Figure 1). There is no correlation or trend between temperature and zircon age.

In addition to calculating the Ti-in-zircon temperature, we can use the whole rock composition to determine the temperature at which the melt would have reached zircon saturation (Boehnke et al., 2013). The range of temperatures that these melts reached saturation is 743–781°C (Figure S6 in Supporting Information S1). We also considered the calibration of Watson and Harrison (1983); however, the range of temperatures calculated is higher



15252027, 2024, 8, Downloaded from https://agupubs.onlinelibrary.wiley.com/doi/10.1029/2024GC011680, Wiley Online Library on [02/02/2025]. See the Terms and Conditions (https://onlinelibrary.wiley.com/terms-and-conditions) on Wiley Online Library for rules of use; OA articles are governed by the applicable Creative Commons License

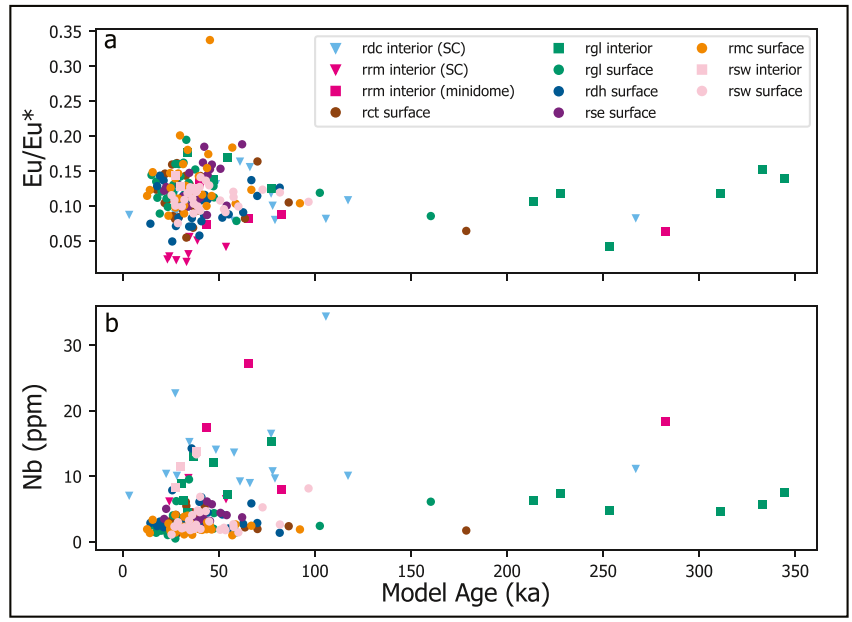


**Figure 5.** Comparison of South Sister zircon crystallization ages to zircon trace element ratios. There are no clear trends between zircon crystal age and composition for these, or other, trace elements. Geologic unit abbreviations are as in Figure 1.

(791–824°C) and are not consistent with the Ti-in-zircon temperature onset as the saturation temperatures using Boehnke et al. (2013). We do not calculate saturation temperatures using Crisp and Berry (2022) because their experiments only go down to 750°C, which is not a low enough temperature for this system, and the model includes $H_2O$ values, which we do not have a constraint for.

## 5. Discussion

### 5.1. Revisited Eruption Chronology and Eruption Rate

#### 5.1.1. Updated Eruption Chronology

In addition to utilizing zircon for information about the magmatic system, zircon surface dates can represent an eruption age if zircon crystallization continued to the time of eruption, and growth was rapid enough to produce a thick enough rim that could be analyzed by an ion probe (~4 μm for $^{230}$Th-$^{230}$U dating). Examples include Lava Creek Tuff in Yellowstone National Park (Matthews et al., 2015) and Wilson Creek Formation of Mono Lake, California (Vazquez & Lidzbarski, 2012).

While a majority of the Pleistocene zircon dates are older than or indistinguishable from the associated $^{40}$Ar/$^{39}$Ar date, in accordance with the typical assumptions of $^{40}$Ar/$^{39}$Ar and $^{238}$U-$^{230}$Th systematics, the weighted mean age of the youngest zircons from rsw and rmc are significantly younger than the corresponding $^{40}$Ar/$^{39}$Ar date at the 1σ level, regardless of the standard used. The $^{40}$Ar/$^{39}$Ar dates for rsw and rmc are plateau ages of bulk plagioclase separates. The low K contents and low radiogenic yields make the ages susceptible to excess Ar—i.e. $^{40}$Ar that is not attributable to in situ decay or atmospheric Ar (Kelley, 2002). The inverse isochron intercepts of the incremental heating experiments for rsw and rmc are within the uncertainty of the $^{40}$Ar/$^{36}$Ar ratio of atmospheric Ar; however, particularly the larger uncertainty of the isochron intercept for rsw may not be sufficiently sensitive to the small quantities of excess $^{40}$Ar needed to produce a spurious date due to the low $^{40}$Ar * yields of the plagioclase separates. Moreover, we note that the incremental heating spectra for rmc are somewhat "saddle shaped" (i.e., the ages of intermediate heating steps are consistently lower than the lower and high temperature heating steps), which is often interpreted as reflecting the presence of excess Ar (Kelley, 2002). It is also possible that inherited plagioclase crystals contributed to the older dates; however, we do not find consistent textural evidence that the plagioclase was inherited, and $^{230}$Th-$^{226}$Ra ages for the two Holocene rhyolites suggest that the plagioclase records near-eruption growth (Stelten & Cooper, 2012).



15252027, 2024, 8, Downloaded from https://agupubs.onlinelibrary.wiley.com/doi/10.1029/2024GC011680, Wiley Online Library on [02/02/2025]. See the Terms and Conditions (https://onlinelibrary.wiley.com/terms-and-conditions) on Wiley Online Library for rules of use; OA articles are governed by the applicable Creative Commons License

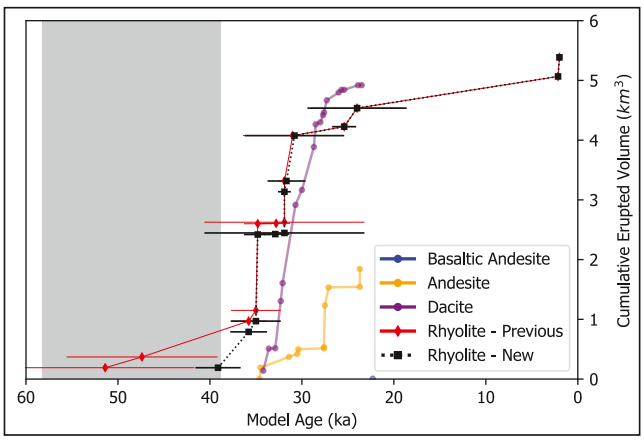


**Figure 6.** Age (ka) and volume ($km^3$) plot of South Sister for all erupted lava types. The *y*-axis shows the cumulative South Sister lava exposed ($km^3$) (Fierstein et al., 2011). The previously adopted timeline (Calvert et al., 2018; Fierstein et al., 2011; Hildreth et al., 2012) suggests South Sister erupted before Middle Sister initiated (gray box, 1$\sigma$) and the first South Sister eruption was 51.39 ka (red diamonds). Our zircon dates suggest that volcanism at South Sister began eruption after Middle Sister and South Sister experienced a higher rate of rhyolite eruptive productivity from 40–30 ka than previously recognized (black squares).

While the $^{40}Ar/^{39}Ar$ plagioclase ages and $^{238}U$-$^{230}Th$ ages overlap at the 95% confidence level, we propose that the more precise, and younger, zircon surface weighted mean dates of 31.5 ± 2.1 and 39.1 ± 2.4 ka for rmc and rsw, respectively, represent the better determinations of the eruption age for these units. Zircon crystallization occurs in the melt body and thus cannot occur after eruption; therefore, the zircon age must be a more accurate representation of eruption age. These younger eruption ages are consistent with field relationships. Because rws and rmc are the oldest known eruptions of South Sister, this revision of their eruption ages inverts the relative timing of the initiation of Pleistocene volcanism at South Sister and Middle Sister and compresses the overall period of cone building at South Sister (Figure 6).

### 5.1.2. Implications of Updated Eruption Chronology

Early work at Three Sisters suggested that North Sister is the oldest of the three, Middle Sister started erupting next, and after Middle Sister was no longer erupting, South Sister's eruptive sequence began (Clark, 1983; Hildreth et al., 2012; Wozniak, 1982). However, new mapping and dating by Fierstein et al. (2011), Hildreth et al. (2012) and Calvert et al. (2018) found that the oldest Middle Sister lava eruption age of 48.5 ± 10 ka (mnf) and the oldest South Sister lava of rsw at 51.4 ± 9.7 ka were of similar age. They concluded that North Sister is still the oldest, but South Sister was the next edifice to be active, followed by Middle Sister as the last edifice to have its first eruption, noting that these dates are not distinguishable, and that activity at South and Middle Sisters largely spanned a similar period in the late Pleistocene. Our revised eruption age for rsw, 39.1 ± 2.4 ka, now postdates the earliest known eruption from Middle Sister (Figure 6) but does not change the broader point that the Pleistocene South Sister and Middle Sister eruptions were largely contemporaneous. Products of earlier eruptions from both edifices that would further refine this timeline may have been removed by glaciation and/or buried, but our new dates indicate that Middle Sister initiated before South Sister. The revised rsw and rmc eruption ages fall in the general pause of Middle Sister activity, ranging from approximately 37 to 27 ka (Fierstein et al., 2011). While Middle Sister and South Sister have overlapping eruptive periods, this shift in the South Sister eruption timeline suggests a higher productivity of silicic eruptions at South Sister while Middle Sister was eruptively quiet.

The new, younger eruption ages of rsw and rmc condense the eruption sequence such that nine rhyolites erupted from 40–30 ka, rather than just seven, increasing the eruptive rate of the system significantly during this timeframe, and all the Pleistocene rhyolites erupted within 15.1 kyr rather than 27.4 kyr. To evaluate the changes in eruptive rate at South Sister due to the revised eruptive sequence, we consider the cone building phase of the late Pleistocene that concluded at ~22 ka (i.e., excluding the Holocene eruptions). Based on the $^{40}Ar/^{39}Ar$ dates, the eruptive rate for all lava types is 0.39 $km^3$/kyr and for rhyolite lava is 0.17 $km^3$/kyr over the cone building stage. However, with the updated eruption ages, the eruptive rate for all lava types is 0.67 $km^3$/kyr and for rhyolite lava is 0.30 $km^3$/kyr over the cone building stage, almost doubling the eruptive rate during this time interval. Calculated for all eruptions over the lifetime of the volcano, the eruptive rate of South Sister is 0.4 $km^3$/kyr, which is a moderate rate compared to other well-characterized Cascade Range volcanoes: Mount Baker is 0.1–0.2 $km^3$/kyr, Mount St. Helens is 2 $km^3$/kyr, Mount Adams is 0.4–0.6 $km^3$/kyr, and Mount Shasta is 0.75 $km^3$/kyr (Hildreth, 2007).

## 5.2. Trace Element Fingerprints of Magma Reservoir Structure

Correlations among zircon trace element compositions are commonly interpreted to reflect the compositional evolution of the host melt resulting from the crystallization or destabilization of zircon or other co-existing phases. The Hf composition is a common index of zircon crystallization, whereby an increase in Hf suggests progressive zircon crystallization (Claiborne et al., 2006; Hoskin & Schaltegger, 2003). Likewise, the Eu anomaly is used as a differentiation index for plagioclase, where a decrease in the Eu/Eu* ratio tracks a melt crystallizing plagioclase, and thus the fractional crystallization of the melt more generally. The partitioning of Ti in a zircon is temperature sensitive and as such, the concentration of Ti in zircon is used to understand the temperature of the



15252027, 2024, 8, Downloaded from https://agupubs.onlinelibrary.wiley.com/doi/10.1029/2024GC011680, Wiley Online Library on [02/02/2025]. See the Terms and Conditions (https://onlinelibrary.wiley.com/terms-and-conditions) on Wiley Online Library for rules of use; OA articles are governed by the applicable Creative Commons License

15252027, 2024, 8, Downloaded from https://agupubs.onlinelibrary.wiley.com/doi/10.1029/2024GC011680, Wiley Online Library on [02/02/2025]. See the Terms and Conditions (https://onlinelibrary.wiley.com/terms-and-conditions) on Wiley Online Library for rules of use; OA articles are governed by the applicable Creative Commons License

system (Ferry & Watson, 2007). Additionally, U has a higher partition coefficient than the still compatible Th, and with high partition coefficients for the heavy rare earth elements (HREE) in zircon, progressive zircon crystallization should also decrease the U/Th ratio and the abundance of HREE relative to middle rare earth elements (MREE) and light rare earth elements (Claiborne et al., 2018; Hoskin & Schaltegger, 2003).

The decrease in Ti and Eu/Eu* with increasing Hf concentrations for the Pleistocene rhyolite's zircon data is consistent with the down-temperature co-crystallization of zircon and plagioclase (Figures 4a and 4c). In contrast to Ti and Eu/Eu*, we do not see a correlation between Hf and the U/Th or REE ratios that would be expected if zircon crystallization was the principal process affecting these ratios (Figure 4e). Moreover, we do not see a zircon crystallization trend in the generally flat U/Th versus Eu/Eu* trend (Figure 4b). However, the U/Th ratio and REE ratios such as Yb/Gd are correlated to each other but not with the indication of zircon crystallization or general crystallization, suggesting that another process exerts greater leverage on the evolution of these elements.

Processes that could also influence these concentrations outside zircon crystallization include the crystallization or destabilization of phases such as amphibole, clinopyroxene, titanite, and/or Fe-Ti oxides. Broadly speaking, clinopyroxene and Fe-Ti oxides do not incorporate U, Th, or the REE in high enough concentrations to have a large impact on their evolution. Importantly, we note that $K_D^{U}/K_D^{Th} < 1$ and $K_D^{MREE}/K_D^{HREE} > 1$ in titanite and amphibole, while $K_D^{U}/K_D^{Th} > 1$ and $K_D^{MREE}/K_D^{HREE} < 1$ in zircon, so crystallization of these phases drives the U/Th and Yb/Gd ratios of the residual melt in opposite directions. The evolution produced by U/Th versus Yb/Gd could be caused by either zircon or titanite/amphibole crystallization. However, the lack of correlation with Hf, the flat U/Th versus Eu/Eu* trend, and the negative correlation between U/Th versus Y/Sc (which is the opposite trend if zircon crystallization were controlling the evolution of these elements, Bachmann et al., 2005) suggests that zircon is not leveraging control of the evolution of these elements. Additionally, we see higher Nb concentrations and Y/Sc ratios at low U/Th ratios that indicate zircon fractionation, but this is not consistent with the whole rock compositional evolution (Hildreth et al., 2012). These data trends rule out zircon crystallization as the main influence on these trace elements so instead, we propose that the trends in U/Th and the REE are consistent with the involvement of amphibole and titanite (Figure 4f).

While the trace element compositions of the surfaces are largely indistinguishable, some zircon interiors are marked by higher concentrations of Nb, Ti, and Sc. Most Nb concentrations are <5 ppm, Ti concentrations are ~2–10 ppm, and Sc concentrations are ~50–100 ppm (Figure 4, Figure S5 in Supporting Information S1). However, the zircon interiors for rgl and rsw reach higher concentrations of 15, 26, and 150 ppm for Nb, Ti, and Sc, respectively. Comparing Y/Sc versus Nb shows two distinct trends: one with lower Nb values and one with higher Nb values (Figure 4g). Nb can be moderately incompatible or compatible in zircon and amphibole but is always compatible in titanite (Bachmann et al., 2005; Berlo et al., 2004; Tiepolo et al., 2007). Due to these differences in the affinity for Nb, we interpret the higher Nb trend to be due to titanite destabilization, and the lower Nb trend to be caused by amphibole destabilization (Bachmann et al., 2005). The high-Nb titanite signature is found more often in zircon interiors.

As such, we suggest that the destabilization of amphibole and titanite in response to magma recharge deeper in the magmatic system is the principal driver of the U, Th, and REE ratios, thereby decoupling them from zircon and plagioclase co-crystallization. Very rare amphibole is present in the Holocene lavas, and its cryptic involvement in the Pleistocene lava is inferred from trace element trends and is a common feature of intermediate to silicic arc magmatic systems more generally (Davidson et al., 2007). While titanite has not been identified in the South Sister lavas, cryptic titanite destabilization in the magma could still contribute to these zircon compositions. Titanite is a common late-stage accessory mineral in felsic calc-alkaline plutons; thus, its presence in the cooler, more crystallized mush would be not surprising (Kohn, 2017).

Various vocabulary and schematics have been postulated to describe the anatomy of the magmatic system beneath a volcano informed by both geophysical and geochemical evidence (e.g., Annen, 2009; Bachmann & Bergantz, 2004; Bacon & Druitt, 1988; Charlier et al., 2005; Cooper & Kent, 2014; Hildreth, 1981, 2004; Huber et al., 2009; Marsh, 1981). Here, we propose a framework involving a mush zone and melt-rich holding chambers. We consider a mush zone located in the upper crust where silicic melts focus and crystalize to a high-crystal content, the crystallinity, longevity, and temperature of which can vary (Dufek & Bachmann, 2010; Hildreth, 2004; Kent & Cooper, 2018). The melt-rich holding chambers represent the melt-segregation from the mush that can more readily be erupted (Bachmann & Bergantz, 2004; Hildreth, 2004). It has been suggested that there is magma distributed throughout the upper crust beneath South Sister (e.g., Brophy & Dreher, 2000;

15252027, 2024, 8, Downloaded from https://agupubs.onlinelibrary.wiley.com/doi/10.1029/2024GC011680, Wiley Online Library on [02/02/2025]. See the Terms and Conditions (https://onlinelibrary.wiley.com/terms-and-conditions) on Wiley Online Library for rules of use; OA articles are governed by the applicable Creative Commons License

Hill, 1991) as well as in the lower crust (e.g., Hildreth, 2007; Hildreth et al., 2012). The presence of rare amphibole in the Holocene rhyolites, but not in the late Pleistocene rhyolites, suggests some level of interconnectivity between a slightly deeper melt body and the shallower, more evolved mush that is tapped for rhyolitic eruption. The common mush zone fingerprints the indistinguishable trace element trends across the Pleistocene eruptions, and the interconnectivity of the magma system provides transport of amphibole and titanite into the crystal mush (Cashman et al., 2017). Periodic intrusions needed to maintain melt in the upper crust (Dufek & Bergantz, 2005; Karakas & Dufek, 2015) may periodically destabilize amphibole and titanite, as recorded by the trace element trends. The resulting melts are then assimilated into the larger magma reservoir. The locus of amphibole and titanite destabilization need not be coincident with in space or time with the zircon crystallization, but apparently was volumetrically significant to dominate the REE and U/Th budget of the magma system.

### 5.3. Integrated Perspective of the Late Pleistocene Magma System

#### 5.3.1. Longevity and Structure

In addition to the trace element fingerprints of the structure of the magma system, we can utilize the zircon dates to consider the longevity of the Pleistocene magma system. The continuity of zircon crystal dates for all Pleistocene rhyolites falling from 100–20 ka suggests a long-lived mush zone of silicic magmas and zircon crystallization. We suggest that this mush zone allowed for the destabilization of amphibole and titanite, catalyzed by new arrivals of more mafic magma from the depth of the interconnected magmatic system and melt-rich holding zones of more readily eruptible material. These holding chambers could be distinct, one getting tapped for each Pleistocene eruption, or more interconnected and tapped over the Pleistocene rhyolite eruptions. The clustering of zircon surface dates around the eruption ages suggests that the magma body remained at zircon saturation composition and temperatures up to eruption or long enough to grow the ∼4 μm zircon depth to be analyzed, suggesting hundreds to thousands of years of storage based on zircon growth and dissolution kinetics (Watson, 1996).

This common mush zone is also supported by the lack of temperature, temporal, or spatial trends in the zircon crystal ages and compositions. We can distinguish neither individual Pleistocene rhyolites nor geographic clusters of eruptions, for example, those east versus west of the summit, based on their zircon trace element compositions. While we do see a range of Eu/Eu* and Yb/Gd ratios, there is no systematic increase or decrease through time to suggest major melt body processes or evolution in the system. Additionally, using the Ti-in-zircon thermometer, we see no thermal correlation with zircon model age. The shortened interval of rhyolite eruptions in the Pleistocene suggested in this work and a lack of temporal or spatial trace element trends supports a single reservoir that was repeatedly tapped over the eruption sequence. Conversely, multiple physically distinct reservoirs could have been tapped and emptied via a single eruption. The zircon data cannot distinguish between a melt-rich or a mushy extraction source. No matter the process of eruption, the mush zone was likely a dynamic system that was continually replenished via the interconnected system but remained constant chemically through the Pleistocene rhyolite eruption sequence.

#### 5.3.2. Regional Connections to the Magma System

In addition to the proposed magma system beneath South Sister, there is evidence of xenocrystic zircons in one eruptive unit from a near-by volcano. While most of the zircon crystal populations range from 100 to 20 ka, Rhyolite of Green Lakes (rgl) includes an older subset of zircon ages ranging from 150 ka to secular equilibrium (>350 ka). The extent of the exposed rgl is on the eastern flank of South Sister with proximity to Broken Top volcano (Figure 1). While other lavas, such as rse and rdc, are also on the eastern flank, rgl has the most complete dataset including both surface and interior zircon analyses. Broken Top eruptive activity lasted from 300 to 150 ka and compositionally ranged from basalt to rhyodacite (Hildreth, 2007). The correlation between the older rgl zircon age population and the Broken Top eruptions suggests that either: (a) rgl inherited xenocrysts from the solidified Broken Top magma system or (b) the Broken Top magma system remained active for more than 100 kyr following the final eruptions of Broken Top and also fed the rgl eruption. Scenario (a) is favored due to the bimodal age distribution of interior zircon model ages (Figures 2 and 3), whereas scenario (b) would have produced a more continuous age distribution from secular equilibrium through to 20 ka. Currently, Broken Top is an understudied volcano. Further mapping, geochronology, and petrologic investigation at Broken Top would allow an improved understanding of its magmatic system and support comparison to that of South Sister. Other volcanic centers in the area such as Todd Lake volcano, Tam McArthur Rim, and the Tumalo volcanic complex

15252027, 2024, 8, Downloaded from https://agupubs.onlinelibrary.wiley.com/doi/10.1029/2024GC011680, Wiley Online Library on [02/02/2025]. See the Terms and Conditions (https://onlinelibrary.wiley.com/terms-and-conditions) on Wiley Online Library for rules of use; OA articles are governed by the applicable Creative Commons License

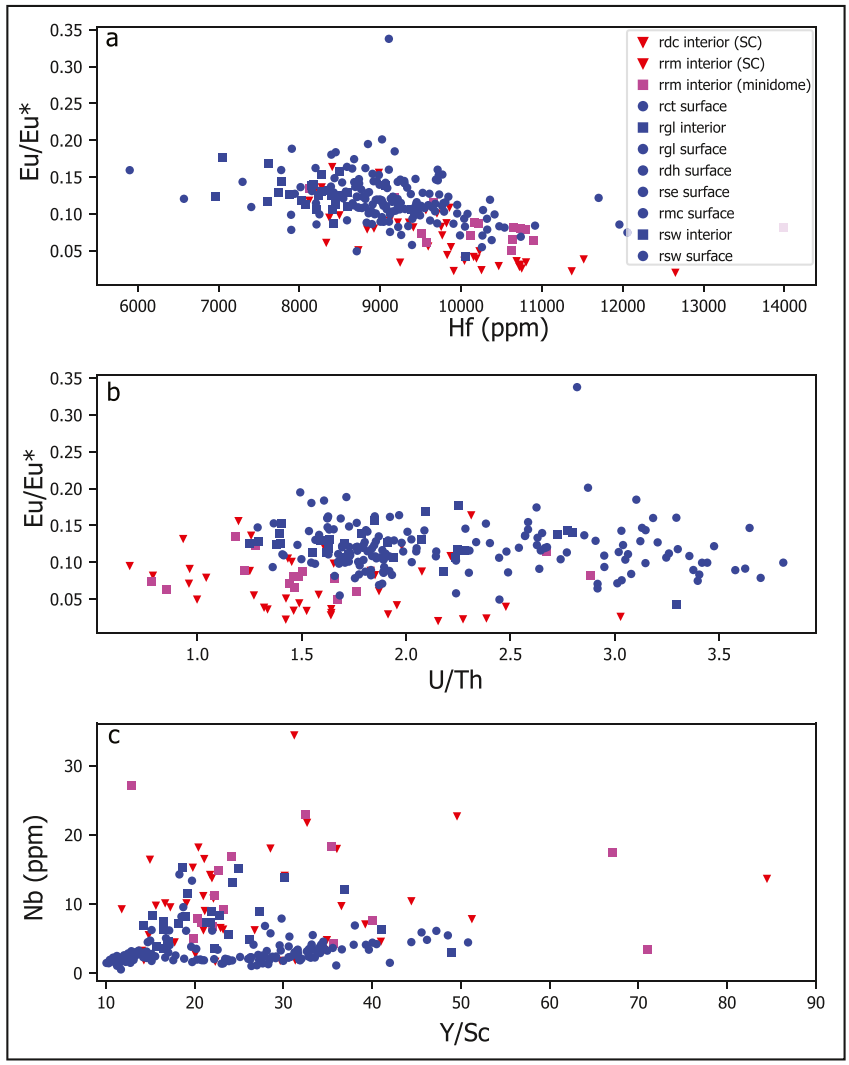


**Figure 7.** Comparison of the trace element compositions and ratios for the main Holocene rhyolite lava (data from Stelten & Cooper, 2012) (red), the rrm mini dome (pink), and the Pleistocene rhyolites (blue). The zircons from the Holocene and Pleistocene lavas can be distinguished based on their trace element compositions, except for the rrm minidome (pink squares), which displays some chemical affinity to both groups, see text. Geologic unit abbreviations are as in Figure 1.

could also be the source of these older zircon crystals; however, the overlapping ages and proximity suggest that Broken Top is the more likely candidate (Hildreth, 2007; Hill, 1991; Klemetti et al., 2023).

### 5.4. Comparing the Late Pleistocene and Holocene Magma Systems

In addition to the Pleistocene data set collected for this project, we can include a comparison of the Holocene data set of Stelten and Cooper (2012) to infer the state of the magmatic system over time. As discussed above, the Pleistocene rhyolites largely cannot be distinguished from one other based on zircon compositions, except for the higher Nb interiors of rgl and rsw. However, zircons from the Holocene rhyolites do show a distinction in compositions when compared to those from the Pleistocene rhyolites (Figure S7 in Supporting Information S1). The highest Nb concentrations occur in the Holocene zircons and the Holocene zircons have predominately lower Eu/Eu* (Figure 7).

This distinction of trace element concentrations between the two main Holocene lavas and the Pleistocene lavas suggests that the mush zone and melt-rich bodies that fed these two eruption sequences are distinct. The overlap in zircon crystal dates from all units implies that the mush zones that fed these eruptions were largely coeval in the

15252027, 2024, 8, Downloaded from https://agupubs.onlinelibrary.wiley.com/doi/10.1029/2024GC011680, Wiley Online Library on [02/02/2025]. See the Terms and Conditions (https://onlinelibrary.wiley.com/terms-and-conditions) on Wiley Online Library for rules of use; OA articles are governed by the applicable Creative Commons License

crust and likely relatively restricted in the spatial area of the system. As such, it is likely that the melt source for the two main Holocene lavas was present during the Pleistocene eruptive sequence but was not tapped for an eruption. These could be two physically distinct melt-rich bodies (e.g., Stelten & Cooper, 2012) or a single body that was tapped for both Holocene eruptions.

Additionally, compared to the late Pleistocene zircon crystals, the Holocene samples tend to have higher Nb compositions, reflecting likely more titanate dissolution (Figure 7c). The erupted Holocene magmas may have been derived from a slightly more fractionated source than the late Pleistocene magmas as suggested by the lower Eu/Eu* ratios. Such constraints could also suggest that the late Pleistocene rhyolites reflect a deeper part of the magmatic system relative to the Holocene rhyolites.

While the compositional distinction between the Pleistocene eruptions and the two main Holocene eruptions is clear, the rrm minidome complicates the story. The rrm minidome is located just east of the main rrm coulee vent and shares compositional trends with both the main Holocene and late Pleistocene groups of lava. In U/Th, Nb, and U, the rrm minidome compositions match that of the Holocene group (Figure S7 in Supporting Information S1). In Eu/Eu* and Ti, the rrm minidome has similar values to the Pleistocene rhyolite zircons. However, there is also considerable overlap between the rrm minidome with both the late Pleistocene and Holocene groups in other compositions. While we do not have enough data to make a concrete conclusion, causation for these trends includes cooling along the edge of the rrm reservoir that erupted as the rrm minidome or the interaction of the rrm reservoir with a remnant of the Pleistocene system.

### 5.5. Holocene Implications

Not only does this work help us understand the evolution and structure of the past rhyolitic magmatic system at South Sister, but it can also give us clues to how a modern rhyolitic magma system could evolve. Specifically, we highlight how the Pleistocene rhyolite eruptive sequence could be repeated in the Holocene. The Pleistocene rhyolite magmas all originated from the common South Sister magmatic system, evolved in a long-lived partially crystallized mush, and erupted from melt-rich region(s) for each eruption. The updated South Sister eruption chronology suggests a higher rhyolitic eruptive rate of 0.30 $km^3$/kyr during the 39–22 ka cone building stage. Notably, the recurrence interval of rhyolitic eruptions from 40 to 30 ka is just over a thousand years, during which nine of the 11 Pleistocene rhyolites erupted.

The inflation at South Sister since the mid-1990s and the spring geochemistry do suggest that magmatism continues beneath South Sister (Evans et al., 2004; Lisowski et al., 2021). Therefore, it must be considered if the Holocene eruptions are the beginning of a cluster of rhyolite eruptions similar to the Pleistocene episode. Continuing and additional efforts such as additional monitoring and geophysical imaging to identify and characterize an active reservoir that could feed multiple future eruptions is currently beneath South Sister would help explain if the late Pleistocene episode is a relevant guide to future volcanism. If so, this would suggest that the eruptive volume, sequences, hazards, and hazard zones from the 40–30 ka eruptions would become an important reference for mitigation and monitoring of future volcanic hazards at South Sister.

## 6. Conclusions

1. The two oldest South Sister rhyolites (rsw and rmc) are 12.3 and 15.9 kyr younger than previously thought, making South Sister the most recent of the Three Sisters to initiate eruptive activity. The resulting shorter duration of the edifice building stage at South Sister almost doubles the eruptive rate during this stage.
2. Zircon compositions record magma evolution by down-temperature plagioclase and zircon co-crystallization. However, they also record the influence of destabilized amphibole and titanite in the magma system. The destabilization of these phases exerted compositional leverage on the U, Th, and REE compositions of the melt and decoupled these elements from the down-temperature zircon and plagioclase crystallization recorded by Hf, Ti, and Eu/Eu*.
3. The Pleistocene rhyolites were derived from a shared crystal mush that imprinted the compositional similarities of all lavas. This mush remained at zircon saturation composition and temperature for hundreds to thousands of years for zircon rim crystallization prior to eruption of the melt-rich region(s).
4. The main flows and domes of the Holocene rhyolites have zircons with similar ages but distinctly lower Eu/Eu* ratios than zircons from the Pleistocene rhyolites, suggesting they crystallized from melts that underwent

more plagioclase fractionation than the Pleistocene rhyolites. As such, these Holocene eruptions come from a separate reservoir or mush body than the Pleistocene eruptions.

5. The Holocene rhyolite eruptive sequence is distinct from the Pleistocene rhyolite eruptive sequence and thus could follow a unique eruptive future. Conversely, the Pleistocene rhyolite eruptive sequence could be repeated in the Holocene. If volcanic history repeats itself, we can expect a rhyolitic eruption recurrence interval of just over a thousand years and an eruptive rate of 0.30 $km^3$/kyr. The Pleistocene rhyolite eruptive sequence is an important reference for evaluating future hazards at South Sister, while acknowledging South Sister could be in a new rhyolitic eruption sequence.

## Data Availability Statement

Data is available through Dechert (2024) and the Zenodo DOI https://doi.org/10.5281/zenodo.12761102 as well as in Supporting Information S1.

**Acknowledgments**
We thank reviewers Erik Klemetti, Mark Stelten, and editor Marie Edmonds for their constructive comments that improved this manuscript. This work is supported by the US NSF (EAR1940994), a Jack Kleinman Memorial Fund for Volcanic Research award, and the USGS Volcano Hazards Program. Lauren Wratchford provided assistance in the field. The Stanford-USGS Micro Analysis Center (RRID:SCR_023252) provided instrument time, technical support, and scientific guidance for acquiring the ion micro probe data presented in this paper. Any use of trade, firm, or product names is for descriptive purposes only and does not imply endorsement by the U.S. Government.

## References

Annen, C. (2009). From plutons to magma chambers: Thermal constraints on the accumulation of eruptible silicic magma in the upper crust. *Earth and Planetary Science Letters*, *284*(3–4), 409–416. https://doi.org/10.1016/j.epsl.2009.05.006

Bachmann, O., & Bergantz, G. W. (2004). On the origin of crystal-poor rhyolites: Extracted from batholithic crystal mushes. *Journal of Petrology*, *45*(8), 1565–1582. https://doi.org/10.1093/petrology/egh019

Bachmann, O., Dungan, M. A., & Bussy, F. (2005). Insights into shallow magmatic processes in large silicic magma bodies: The trace element record in the Fish Canyon magma body, Colorado. *Contributions to Mineralogy and Petrology*, *149*(3), 338–349. https://doi.org/10.1007/s00410-005-0653-z

Bacon, C. R., & Druitt, T. H. (1988). Compositional evolution of the zoned calcalkaline magma chamber of Mount Mazama, Crater Lake, Oregon. *Contributions to Mineralogy and Petrology*, *98*(2), 224–256. https://doi.org/10.1007/BF00402114

Bacon, C. R., & Lowenstern, J. (2005). Late Pleistocene granodiorite source for recycled zircon and phenocrysts in rhyodacite lava at Crater Lake, Oregon. *Earth and Planetary Science Letters*, *233*(3–4), 277–293. https://doi.org/10.1016/j.epsl.2005.02.012

Berlo, K., Turner, S., Blundy, J., & Hawkesworth, C. (2004). The extent of U-series disequilibria produced during partial melting of the lower crust with implications for the formation of the Mount St. Helens dacites. *Contributions to Mineralogy and Petrology*, *148*(1), 122–130. https://doi.org/10.1007/s00410-004-0590-2

Boehnke, P., Barboni, M., & Bell, E. A. (2016). Zircon U/Th model ages in the presence of melt heterogeneity. *Quaternary Geochronology*, *34*, 69–74. https://doi.org/10.1016/j.quageo.2016.03.005

Boehnke, P., Watson, E. B., Trail, D., Harrison, T. M., & Schmitt, A. K. (2013). Zircon saturation re-revisited. *Chemical Geology*, *351*, 324–334. https://doi.org/10.1016/j.chemgeo.2013.05.028

Brophy, J. G., & Dreher, S. T. (2000). The origin of composition gaps at South Sister volcano, central Oregon: Implications for fractional crystallization processes beneath active calc-alkaline volcanoes. *Journal of Volcanology and Geothermal Research*, *102*(3–4), 287–307. https://doi.org/10.1016/S0377-0273(00)00192-X

Calvert, A. T., Fierstein, J., & Hildreth, W. (2018). Eruptive history of Middle sister, Oregon Cascades, USA-product of a late Pleistocene eruptive episode. *Geosphere*, *14*(5), 2118–2139. https://doi.org/10.1130/GES01638.1

Cashman, K. V., Sparks, R. S. J., & Blundy, J. D. (2017). Vertically extensive and unstable magmatic systems: A unified view of igneous processes. *Science*, *355*(6331), eaag3055. https://doi.org/10.1126/science.aag3055

Charlier, B. L. A., Wilson, C. J. N., Lowenstern, J. B., Blake, S., Van Calsteren, P. W., & Davidson, J. P. (2005). Magma generation at a large, hyperactive silicic volcano (Taupo, New Zealand) revealed by U–Th and U–Pb systematics in zircons. *Journal of Petrology*, *46*(1), 3–32. https://doi.org/10.1093/petrology/egh060

Cheng, C., Bodin, T., Tauzin, B., & Allen, R. M. (2017). Cascadia subduction slab heterogeneity revealed by three-dimensional receiver function Kirchhoff migration. *Geophysical Research Letters*, *44*(2), 694–701. https://doi.org/10.1002/2016GL072142

Cheng, H., Edwards, R. L., Hoff, J., Gallup, C. D., Richards, D. A., & Asmerom, Y. (2000). The half-lives of uranium-234 and thorium-230. *Chemical Geology*, *169*(1–2), 17–33. https://doi.org/10.1016/S0009-2541(99)00157-6

Cheng, H., Lawrence Edwards, R., Shen, C.-C., Polyak, V. J., Asmerom, Y., Woodhead, J., et al. (2013). Improvements in 230Th dating, 230Th and 234U half-life values, and U–Th isotopic measurements by multi-collector inductively coupled plasma mass spectrometry. *Earth and Planetary Science Letters*, *371–372*, 82–91. https://doi.org/10.1016/j.epsl.2013.04.006

Claiborne, L. L., Miller, C. F., Flanagan, D. M., Clynne, M. A., & Wooden, J. L. (2010). Zircon reveals protracted magma storage and recycling beneath Mount St. Helens. *Geology*, *38*(11), 1011–1014. https://doi.org/10.1130/G31285.1

Claiborne, L. L., Miller, C. F., Gualda, G. A. R., Carley, T. L., Covey, A. K., Wooden, J. L., & Fleming, M. A. (2018). Zircon as magma monitor: Robust, temperature-dependent partition coefficients from glass and zircon surface and rim measurements from natural systems. In D. E. Moser, F. Corfu, J. R. Darling, S. M. Reddy, & K. Tait (Eds.), *Geophysical monograph series* (1st ed., pp. 1–33). Wiley. https://doi.org/10.1002/9781119227250.ch1

Claiborne, L. L., Miller, C. F., Walker, B. A., Wooden, J. L., Mazdab, F. K., & Bea, F. (2006). Tracking magmatic processes through Zr/Hf ratios in rocks and Hf and Ti zoning in zircons: An example from the Spirit Mountain batholith, Nevada. *Mineralogical Magazine*, *70*(5), 517–543. https://doi.org/10.1180/0026461067050348

Clark, J. G. (1983). *Geology and petrology of South Sister volcano, high Cascades range, Oregon [Ph.D. Dissertation]*. University of Oregon.

Coble, M. A., Vazquez, J. A., Barth, A. P., Wooden, J., Burns, D., Kylander-Clark, A., et al. (2018). Trace element characterisation of MAD-559 zircon reference material for ion microprobe analysis. *Geostandards and Geoanalytical Research*, *42*(4), 481–497. https://doi.org/10.1111/ggr.12238

Cooper, K. M. (2015). Timescales of crustal magma reservoir processes: Insights from U-series crystal ages. *Geological Society, London, Special Publications*, *422*(1), 141–174. https://doi.org/10.1144/SP422.7

Cooper, K. M., & Kent, A. J. R. (2014). Rapid remobilization of magmatic crystals kept in cold storage. *Nature*, *506*(7489), 480–483. https://doi.org/10.1038/nature12991



15252027, 2024, 8, Downloaded from https://agupubs.onlinelibrary.wiley.com/doi/10.1029/2024GC011680, Wiley Online Library on [02/02/2025]. See the Terms and Conditions (https://onlinelibrary.wiley.com/terms-and-conditions) on Wiley Online Library for rules of use; OA articles are governed by the applicable Creative Commons License

Crisp, L. J., & Berry, A. J. (2022). A new model for zircon saturation in silicate melts. *Contributions to Mineralogy and Petrology*, *177*(7), 71. https://doi.org/10.1007/s00410-022-01925-6

Davidson, J., Turner, S., Handley, H., Macpherson, C., & Dosseto, A. (2007). Amphibole "sponge" in arc crust? *Geology*, *35*(9), 787. https://doi.org/10.1130/G23637A.1

Dechert, A. (2024). Zircon constraints on the eruptive sequence and magma evolution of rhyolites at South Sister volcano, Oregon [Dataset]. *Geochemistry, Geophysics, Geosystems. Zenodo*. https://doi.org/10.5281/zenodo.12761102

Dufek, J., & Bachmann, O. (2010). Quantum magmatism: Magmatic compositional gaps generated by melt-crystal dynamics. *Geology*, *38*(8), 687–690. https://doi.org/10.1130/G30831.1

Dufek, J., & Bergantz, G. W. (2005). Lower crustal magma Genesis and preservation: A stochastic framework for the evaluation of basalt–crust interaction. *Journal of Petrology*, *46*(11), 2167–2195. https://doi.org/10.1093/petrology/egi049

Dzurisin, D., Lisowski, M., & Wicks, C. W. (2009). Continuing inflation at Three Sisters volcanic center, central Oregon Cascade Range, USA, from GPS, leveling, and InSAR observations. *Bulletin of Volcanology*, *71*(10), 1091–1110. https://doi.org/10.1007/s00445-009-0296-4

Evans, W. C., van Soest, M. C., Mariner, R. H., Hurwitz, S., Ingebritsen, S. E., Wicks, C. W., & Schmidt, M. E. (2004). Magmatic intrusion west of Three Sisters, central Oregon, USA: The perspective from spring geochemistry. *Geology*, *32*(1), 69. https://doi.org/10.1130/G19974.1

Ewert, J., Diefenbach, A., & Ramsey, D. (2018). *2018 update to the U.S. Geological Survey National volcanic threat assessment (scientific investigations report 2018–5140; scientific investigations report)*. U.S. Department of the Interior.

Ferry, J. M., & Watson, E. B. (2007). New thermodynamic models and revised calibrations for the Ti-in-zircon and Zr-in-rutile thermometers. *Contributions to Mineralogy and Petrology*, *154*(4), 429–437. https://doi.org/10.1007/s00410-007-0201-0

Fierstein, J., Hildreth, W., & Calvert, A. T. (2011). Eruptive history of South Sister, Oregon Cascades. *Journal of Volcanology and Geothermal Research*, *207*(3–4), 145–179. https://doi.org/10.1016/j.jvolgeores.2011.06.003

Finch, R. J., & Hanchar, J. M. (2003). Structure and chemistry of zircon and zircon-group minerals. *Reviews in Mineralogy and Geochemistry*, *53*, 1–26.

Fleck, R. J., Calvert, A. T., Coble, M. A., Wooden, J. L., Hodges, K., Hayden, L. A., et al. (2019). Characterization of the rhyolite of Bodie Hills and $^{40}Ar/^{39}Ar$ intercalibration with Ar mineral standards. *Chemical Geology*, *525*, 282–302. https://doi.org/10.1016/j.chemgeo.2019.07.022

Gardner, C. A. (1994). *Temporal, spatial and petrologic variations of lava flows from the mount Bachelor volcanic chain, central Oregon high Cascades (Open-File report 94-261)*. U.S. Department of the Interior, U.S. Geological Survey.

Hildreth, W. (1981). Gradients in silicic magma chambers: Implications for lithospheric magmatism. *Journal of Geophysical Research*, *86*(B11), 10153–10192. https://doi.org/10.1029/JB086iB11p10153

Hildreth, W. (2004). Volcanological perspectives on long valley, Mammoth mountain, and Mono craters: Several contiguous but discrete systems. *Journal of Volcanology and Geothermal Research*, *136*(3–4), 169–198. https://doi.org/10.1016/j.jvolgeores.2004.05.019

Hildreth, W. (2007). *Quaternary magmatism in the Cascades—Geologic perspectives (professional paper 1744)*. U.S. Department of the Interior, U.S. Geological Survey.

Hildreth, W., Fierstein, J., & Calvert, A. T. (2012). *Geologic map of three Sisters volcanic cluster, cascade range, Oregon (scientific investigations map 3186)* (Vol. 111). U.S. Department of the Interior, U.S. Geological Survey.

Hill, B. (1991). *Petrogenesis of compositionally distinct silicic volcanoes in the three Sisters region of the Oregon Cascade range: The effects of crustal extension on the development of continental arc silicic magmatism. Doctoral dissertation*. Oregon State University.

Hoskin, P. W. O., & Schaltegger, U. (2003). The composition of zircon and igneous and metamorphic petrogenesis. *Reviews in Mineralogy and Geochemistry*, *53*(1), 27–62. https://doi.org/10.2113/0530027

Huber, C., Bachmann, O., & Manga, M. (2009). Homogenization processes in silicic magma chambers by stirring and mushification (latent heat buffering). *Earth and Planetary Science Letters*, *283*(1–4), 38–47. https://doi.org/10.1016/j.epsl.2009.03.029

Ireland, T. R., & Williams, I. S. (2003). Considerations in zircon geochronology by SIMS. *Reviews in Mineralogy and Geochemistry*, *53*(1), 215–241. https://doi.org/10.2113/0530215

Karakas, O., & Dufek, J. (2015). Melt evolution and residence in extending crust: Thermal modeling of the crust and crustal magmas. *Earth and Planetary Science Letters*, *425*, 131–144. https://doi.org/10.1016/j.epsl.2015.06.001

Kelley, S. (2002). K-Ar and Ar-Ar dating. *Reviews in Mineralogy and Geochemistry*, *47*(1), 785–818. https://doi.org/10.2138/rmg.2002.47.17

Kent, A. J. R., & Cooper, K. M. (2018). How well do zircons record the thermal evolution of magmatic systems? *Geology*, *46*(2), 111–114. https://doi.org/10.1130/G39690.1

Klemetti, E. W., & Clynne, M. A. (2014). Localized rejuvenation of a crystal mush recorded in zircon temporal and compositional variation at the lassen volcanic center, northern California. *PLoS One*, *9*(12), e113157. https://doi.org/10.1371/journal.pone.0113157

Klemetti, E. W., Kent, A., McLeod, J., Van Horn, B., Scroggs, A., Campanelli, C., et al. (2023). Evolution of silicic magmatism in the Tumalo volcanic center and three sisters region of the central Oregon Cascades documented through zircon petrochronology. *Geological Society of America Abstracts with Programs*, *55*, 395753. https://doi.org/10.1130/abs/2023AM-395753

Kohn, M. J. (2017). Titanite petrochronology. *Reviews in Mineralogy and Geochemistry*, *83*(1), 419–441. https://doi.org/10.2138/rmg.2017.83.13

Lisowski, M., McCaffrey, R., Wicks, C. W., & Dzurisin, D. (2021). Geodetic constraints on a 25-year magmatic inflation episode near three sisters, central Oregon. *Journal of Geophysical Research: Solid Earth*, *126*(12), e2021JB022360. https://doi.org/10.1029/2021JB022360

Marsh, B. D. (1981). On the crystallinity, probability of occurrence, and rheology of lava and magma. *Contributions to Mineralogy and Petrology*, *78*(1), 85–98. https://doi.org/10.1007/BF00371146

Matthews, N. E., Vazquez, J. A., & Calvert, A. T. (2015). Age of the Lava Creek supereruption and magma chamber assembly at Yellowstone based on $^{40}Ar/^{39}Ar$ and U-Pb dating of sanidine and zircon crystals: Age of the Lava Creek Supereruption. *Geochemistry, Geophysics, Geosystems*, *16*(8), 2508–2528. https://doi.org/10.1002/2015GC005881

McCrory, P. A., Blair, J. L., Waldhauser, F., & Oppenheimer, D. H. (2012). Juan de Fuca slab geometry and its relation to Wadati-Benioff zone seismicity: JDF slab geometry and WBZ seismicity. *Journal of Geophysical Research*, *117*, B9. https://doi.org/10.1029/2012JB009407

Mercer, C. M., & Hodges, K. V. (2016). ArAR—A software tool to promote the robust comparison of K–Ar and $^{40}Ar/^{39}Ar$ dates published using different decay, isotopic, and monitor-age parameters. *Chemical Geology*, *440*, 148–163. https://doi.org/10.1016/j.chemgeo.2016.06.020

Min, K., Mundil, R., Renne, P. R., & Ludwig, K. R. (2000). A test for systematic errors in $^{40}Ar/^{39}Ar$ geochronology through comparison with U/Pb analysis of a 1.1-Ga rhyolite. *Geochimica et Cosmochimica Acta*, *64*(1), 73–98. https://doi.org/10.1016/S0016-7037(99)00204-5

Obrebski, M., Allen, R. M., Xue, M., & Hung, S.-H. (2010). Slab-plume interaction beneath the Pacific Northwest: Western U.S. Seismic tomography. *Geophysical Research Letters*, *37*(14), L14305. https://doi.org/10.1029/2010GL043489

Parker, D. F., Price, J. D., Brooks, C. B., & Ren, M. (2023). Contrasting magmatic evolutions of the Three Sister Volcanoes reflect increased heat flow, crustal melting and silicic magmatism in the Central Oregon Cascade Arc. *Chemical Geology*, *618*, 121294. https://doi.org/10.1016/j.chemgeo.2022.121294



15252027, 2024, 8, Downloaded from https://agupubs.onlinelibrary.wiley.com/doi/10.1029/2024GC011680, Wiley Online Library on [02/02/2025]. See the Terms and Conditions (https://onlinelibrary.wiley.com/terms-and-conditions) on Wiley Online Library for rules of use; OA articles are governed by the applicable Creative Commons License

Reid, M. R., Coath, C. D., Mark Harrison, T., & McKeegan, K. D. (1997). Prolonged residence times for the youngest rhyolites associated with long valley Caldera: $^{230}$Th-$^{238}$U ion microprobe dating of young zircons. *Earth and Planetary Science Letters*, *150*(1–2), 27–39. https://doi.org/10.1016/S0012-821X(97)00077-0

Riddick, S. N., & Schmidt, D. A. (2011). Time-dependent changes in volcanic inflation rate near three sisters, Oregon, revealed by InSAR: Three sisters time-dependent inflation. *Geochemistry, Geophysics, Geosystems*, *12*(12), Q12005. https://doi.org/10.1029/2011GC003826

Rubin, A. E., Cooper, K. M., Till, C. B., Kent, A. J. R., Costa, F., Bose, M., et al. (2017). Rapid cooling and cold storage in a silicic magma reservoir recorded in individual crystals. *Science*, *356*(6343), 1154–1156. https://doi.org/10.1126/science.aam8720

Schaen, A. J., Jicha, B. R., Hodges, K. V., Vermeesch, P., Stelten, M. E., Mercer, C. M., et al. (2021). Interpreting and reporting $^{40}$Ar/$^{39}$Ar geochronologic data. *GSA Bulletin*, *133*(3–4), 461–487. https://doi.org/10.1130/B35560.1

Schmidt, M. E., & Grunder, A. L. (2009). The evolution of North Sister: A volcano shaped by extension and ice in the central Oregon Cascade Arc. *Geological Society of America Bulletin*, *121*(5–6), 643–662. https://doi.org/10.1130/B26442.1

Scott, W. E. (1987). Holocene rhyodacite eruptions on the flanks of South Sister volcano, Oregon. In *Geological society of America special papers* (Vol. 212, pp. 35–54). Geological Society of America. https://doi.org/10.1130/SPE212-p35

Scott, W. E., Iverson, R. M., & Fisher, B. J. (2001). *Volcano hazards in the three Sisters region, Oregon [Open-File report 99-437]*. U.S. Department of the Interior, U.S. Geological Survey.

Sherrod, D. R., Taylor, E. M., Ferns, M. L., Scott, W. E., Conrey, R. M., & Smith, G. A. (2004). Geologic map of the Bend 30-X 60-minute quadrangle, central Orego [map].

Simon, J., & Reid, M. (2005). The pace of rhyolite differentiation and storage in an 'archetypical' silicic magma system, Long Valley, California. *Earth and Planetary Science Letters*, *235*(1–2), 123–140. https://doi.org/10.1016/j.epsl.2005.03.013

Stelten, M. E., & Cooper, K. M. (2012). Constraints on the nature of the subvolcanic reservoir at South Sister volcano, Oregon from U-series dating combined with sub-crystal trace-element analysis of plagioclase and zircon. *Earth and Planetary Science Letters*, *313–314*, 1–11. https://doi.org/10.1016/j.epsl.2011.10.035

Tiepolo, M., Oberti, R., Zanetti, A., Vannucci, R., & Foley, S. F. (2007). Trace-element partitioning between amphibole and silicate melt. *Reviews in Mineralogy and Geochemistry*, *67*(1), 417–452. https://doi.org/10.2138/rmg.2007.67.11

Vazquez, J. A., & Lidzbarski, M. I. (2012). High-resolution tephrochronology of the Wilson Creek Formation (Mono Lake, California) and Laschamp event using 238U-230Th SIMS dating of accessory mineral rims. *Earth and Planetary Science Letters*, *357–358*, 54–67. https://doi.org/10.1016/j.epsl.2012.09.013

Waters, L. E., Andrews, B. J., & Frey, H. M. (2021). Daly gaps at South Sister, Oregon, USA, generated via partial melting. *Contributions to Mineralogy and Petrology*, *176*(7), 52. https://doi.org/10.1007/s00410-021-01805-5

Watson, E. B. (1996). Dissolution, growth and survival of zircons during crustal fusion: Kinetic principals, geological models and implications for isotopic inheritance. *Earth and Environmental Science Transactions of the Royal Society of Edinburgh*, *87*(1–2), 43–56. https://doi.org/10.1017/S0263593300006465

Watson, E. B., & Harrison, T. M. (1983). Zircon saturation revisited: Temperature and composition effects in a variety of crustal magma types. *Earth and Planetary Science Letters*, *64*(2), 295–304. https://doi.org/10.1016/0012-821X(83)90211-X

Wicks, C. W., Dzurisin, D., Ingebritsen, S., Thatcher, W., Lu, Z., & Iverson, J. (2002). Magmatic activity beneath the quiescent Three Sisters volcanic center, central Oregon Cascade Range, USA. *Geophysical Research Letters*, *29*(7), 1122. https://doi.org/10.1029/2001GL014205

Williams, I. S. (1997). U-Th-Pb geochronology by ion microprobe. In *Applications of Microanalytical techniques to understanding mineralizing processes* (Vol. 7, pp. 1–35). Society of Economic Geologists. https://doi.org/10.5382/Rev.07.01

Wozniak, K. C. (1982). *Geology of the northern part of the Southeast Three Sisters quadrangle, Oregon [M.S. thesis]*. Oregon State University.

## References From the Supporting Information

Crowley, J. L., Schoene, B., & Bowring, S. A. (2007). U-Pb dating of zircon in the Bishop Tuff at the millennial scale. *Geology*, *35*(12), 1123. https://doi.org/10.1130/G24017A.1

Gualda, G. A. R., Ghiorso, M. S., Lemons, R. V., & Carley, T. L. (2012). Rhyolite-MELTS: A modified calibration of melts optimized for silica-rich, fluid-bearing magmatic systems. *Journal of Petrology*, *53*(5), 875–890. https://doi.org/10.1093/petrology/egr080

Hayden, L. A., & Watson, E. B. (2007). Rutile saturation in hydrous siliceous melts and its bearing on Ti-thermometry of quartz and zircon. *Earth and Planetary Science Letters*, *258*(3–4), 561–568. https://doi.org/10.1016/j.epsl.2007.04.020

Ludwig, K. R. (2001). Squid (1.13b), A users manual.

Ludwig, K. R. (2003). Isoplot (3.41d), A geochronological toolkit for Excel.

McDonough, W. F., & Sun, S. S. (1995). Composition of the Earth. *Chemical Geology*, *120*(3–4), 223–253. https://doi.org/10.1016/0009-2541(94)00140-4

Watson, E. B., Wark, D. A., & Thomas, J. B. (2006). Crystallization thermometers for zircon and rutile. *Contributions to Mineralogy and Petrology*, *151*(4), 413–433. https://doi.org/10.1007/s00410-006-0068-5



15252027, 2024, 8, Downloaded from https://agupubs.onlinelibrary.wiley.com/doi/10.1029/2024GC011680, Wiley Online Library on [02/02/2025]. See the Terms and Conditions (https://onlinelibrary.wiley.com/terms-and-conditions) on Wiley Online Library for rules of use; OA articles are governed by the applicable Creative Commons License